Letter | Editors' Suggestion

Electronic excitation spectra of molecular hydrogen in phase I from quantum Monte Carlo and many-body perturbation methods

Vitaly Gorelov
LSI, CNRS, CEA/DRF/IRAMIS, École Polytechnique, Institut Polytechnique de Paris, F-91120 Palaiseau, France and European Theoretical Spectroscopy Facility (ETSF)

Markus Holzmann
Univ. Grenoble Alpes, CNRS, LPMMC, 38000 Grenoble, France

David M. Ceperley
Department of Physics, University of Illinois Urbana-Champaign, Urbana, Illinois 61801, USA

Carlo Pierleoni
Department of Physical and Chemical Sciences, University of L'Aquila, Via Vetoio 10, I-67010 L'Aquila, Italy

(Received 16 November 2023; revised 13 February 2024; accepted 17 May 2024; published 11 June 2024)

We study the electronic excitation spectra in solid molecular hydrogen (phase I) at ambient temperature and 5- to 90-GPa pressures using quantum Monte Carlo methods and many-body perturbation theory. In this range, the system changes from a wide-gap molecular insulator to a semiconductor, altering the nature of the excitations from localized to delocalized. Computed gaps and spectra agree with experiments, proving the ability to predict accurately band gaps of many-body systems in the presence of nuclear quantum and thermal effects.

DOI: 10.1103/PhysRevB.109.L241111

Introduction. Many-body hydrogen is a fundamental system whose physical properties have been the subject of numerous theoretical and experimental studies. Despite more than a century of investigations, its phase diagram under pressure is still uncertain because of experimental difficulties and computation inaccuracies [1–3]. Of the many crystalline phases detected so far, only the crystalline structures of phases I, III, and IV have been identified by x-ray diffraction [4–6], while the structures of other phases have been predicted based on numerical algorithms [7–9]. Similarly, characterization of the electronic properties, such as energy gaps and excitations, has been achieved mainly by optical probes, like absorption [4,10] and reflection [11] or by transport measurements [12]. In the search for metallic hydrogen, the electronic gap has been measured as a function of increasing pressure. Recently, thanks to progress in high-brilliance x-ray sources and in high-pressure experimental techniques [13–15], inelastic x-ray scattering (IXS) has been successfully employed to detect the electronic excitation spectrum and extract the value of the electronic gap from the lower limit of the photon energy-loss spectra in phase I [16]. From the theoretical perspective, the accurate calculation of optical properties and band gaps is difficult [2], since electron-phonon coupling and excitonic effects are expected to play important roles.

Here we present a detailed theoretical *ab initio* study of the electronic excitation (absorption) spectra of phase I hydrogen based on quantum Monte Carlo (QMC) and many-body perturbation theory (MBPT) methods [17]. Quantum and thermal effects of the protons are included using path-integral Monte Carlo calculations within the Born-Oppenheimer approximation. Whereas the QMC calculations focus on the value of the minimum excitation gap, we also compute the energy-loss spectra based on the Bethe-Salpeter equation (BSE) to directly compare to experimental measurements. Our calculations show that quantum nuclear effects reduce the gap by ∼2 eV, a decrease only weakly dependant on pressure, in contrast to excitonic effects which decrease more rapidly with pressure from ∼2 eV at threefold compression to ∼0.5 eV at 90 GPa (∼ninefold compression). Overall agreement, reported in Fig. 1, is observed between the QMC and BSE calculations and experiment. The remaining small deviations with respect to the experimental values can be attributed to the extrapolation procedure, in particular, the background subtraction used to determine the energy gap from the experimental spectra.

Our results clearly point out the limitations of self-consistent single-electron theories like density functional theory (DFT). Although Ref. [16] reports DFT gaps with the HSE functional in agreement with experimental values, those calculations, based on ideal crystal structures, rely on large error cancellations between the quantum nuclear effects and the systematic underestimation of band gaps of the DFT functional underlying the calculations (see the Supplemental Material of Ref. [16]). In addition, those calculations do not predict the changes between hydrogen and deuterium and the strong pressure dependence of excitonic effects.

Previous MBPT [18–21] or QMC [22–25] studies of excitation gaps or optical properties have mostly focused on the high-pressure regime close to metallization. Since direct experimental results on structural properties are lacking in this region, comparisons with experimental spectra [10] are less conclusive. Further, from a theoretical point of view, most

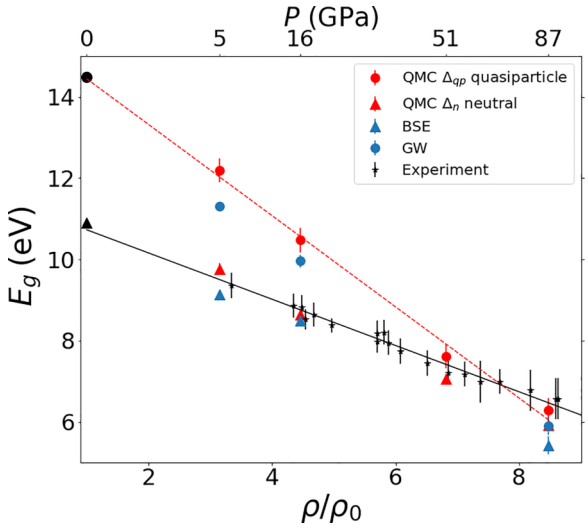

FIG. 1. Comparison between the room-temperature experimental data of Ref. [16] and theoretical predictions for the electronic gap of solid hydrogen in phase I as a function of compression. We report quasiparticle (circles) and neutral gap from QMC (triangles) (red symbols) and from MBPT (blue symbols, triangles BSE, circles GW), both corrected for finite-size effects. The black triangle and the black circle corresponds to the first exciton transition and the interband gap extracted from experimental absorption spectra at zero pressure $\rho/\rho_0 = 1$. The difference between the quasiparticle gap and the neutral gap is the exciton binding energy. The solid black line is a fit to the experimental data; the red dashed line is a fit to the QMC-QP gaps.

of the studies are not fully satisfying; Refs. [18–21,24] completely neglect quantum nuclear motion, whereas Ref. [25] is based on QMC energies for the ideal structures augmented by DFT calculations for phonons in the self-consistent harmonic approximation and electronic excitation spectra using different functionals.

Methods. Phase I of hydrogen has molecular centers on an hcp lattice with molecular orientations being nearly isotropic. This phase is well characterized by x-ray diffraction at room temperature up to 120 GPa [4]. A recent investigation extended the pressure range to phase III and phase IV up to 254 GPa [5], also providing the equation of state (EOS) and the cell geometry.

For our numerical study, we consider hydrogen molecules in the $P6_3/m$ structure with four molecules per unit cell. As in previous studies of hydrogen [23,26], we employed a supercell with 48 molecules ($N = 96$ protons) comprising $3 \times 2 \times 2$ conventional cells (orthorhombic), a workable compromise between supercells with nearly cubic shape and a modest number of atoms. Molecules in the supercell were randomly oriented corresponding to the situation of phase I at room temperature [26]. We performed structural optimization of the molecular positions and supercell geometry at constant stress using the vdW-DF1 functional within DFT. This functional is among the best functionals for high-pressure molecular hydrogen as benchmarked against QMC predictions [27,28]. After geometry optimization we performed a room temperature NVT-Smart Monte Carlo simulation with both classical and quantum protons, employing energies and forces from the DFT-vdW-DF1 functional to generate a set of uncorrelated configurations.

This procedure was repeated at four different densities corresponding to compression values $\rho/\rho_0 = 3.15$, 4.47, 6.86, and 8.48 ($r_s = 2.21$, 1.97, 1.71, and 1.59, respectively) in order to investigate the pressure range between 5 and 90 GPa. Here $\rho_0 = 0.0396$ g/cm^3 is the reference density at ambient pressure and cryogenic temperature. Since the molecular geometry using DFT-vdW-DF1 are found to be accurate [27,28], we did not use the more expensive CEIMC algorithm (which relies on the QMC energies) for optimization. Details of the thermodynamics and structures are reported in the Supplemental Material [29] (see also Refs. [4,16,30–56] therein).

At each density and for each different system, we selected 20 independent configurations for the calculations of the electronic excitations within QMC, 10 of which were also employed in the BSE calculations. Electronic energies were first averaged over the nuclear configurations and excitation gaps were obtained from the difference of averaged energies (see the Supplemental Material [29] for details). Such a quantum average procedure becomes exact at low temperatures where zero point motion dominates the nuclear trajectories as is the case for hydrogen at $T = 300$K [22,57].

For each nuclear configuration, we first computed the fundamental or quasiparticle gap as

$$\Delta_{qp} = E_0(N_e + 1) + E_0(N_e - 1) - 2E_0(N_e), \qquad (1)$$

adding and removing up to 6 electrons using reptation QMC (RQMC) with a uniform positive background charge to have charge neutrality in the supercell. To account for finite-size effects, we have used grand canonical twist averaging (GCTABC) and corrected for the leading-order size effects according to $\Delta_{qp}^{\infty} - \Delta_{qp}^{L} = |v_M(L)|/\epsilon$ as described in Ref. [40]. Here, $v_M(L) \sim 1/L$, the Madelung constant (reported in the table in the Supplemental Material [29]), and L is the extension of the nearly cubic supercell. Heuristically, this $1/L$ dependence of the quasiparticle gap can be attributed to the additional charge interactions of the doped systems [58,59]. For all QMC calculations, the dielectric constant ϵ used for size corrections has been extracted from extrapolating the long-range behavior of the structure factor (see the Supplemental Material [29]).

As a second step, we also computed the neutral electron-hole gap as

$$\Delta_n = E_1(N_e) - E_0(N_e), \qquad (2)$$

where $E_0(N_e)$ and $E_1(N_e)$ indicate electronic ground and first excited energies with N_e electrons, respectively. In practice, Δ_n is obtained within RQMC by promoting a single Bloch orbital from the ground state to an excited state in the Slater determinant of the trial wave function [60]. Kohn-Sham DFT energies are used to determine the ordering.

Accounting for the finite-size effects of neutral excitations is more delicate. For a fixed number of electrons, the $1/L$ dependence will be absent for neutral excitations for a sufficiently large supercell, since an electron and a hole will be bound together forming a neutral object. In practice, an apparent $1/L$ behavior is still observed [60,61] in situations where the electron-hole attraction is not sufficiently strong, so that the size of the exciton is larger or comparable with

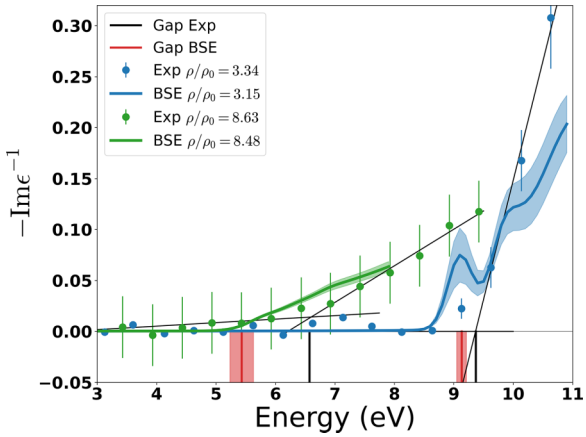

FIG. 2. Comparison of the measured and calculated (BSE) IXS spectra for the lowest (blue) and highest (green) calculated compressions. Closed circles with error bars are experimental data. Straight black lines are fits to the experimental data. Vertical black lines indicate the band gap extracted from the crossing of the fits at the two compressions. The vertical red lines correspond to the BSE neutral gap for the corresponding compression. Only converged parts of the BSE spectra are shown.

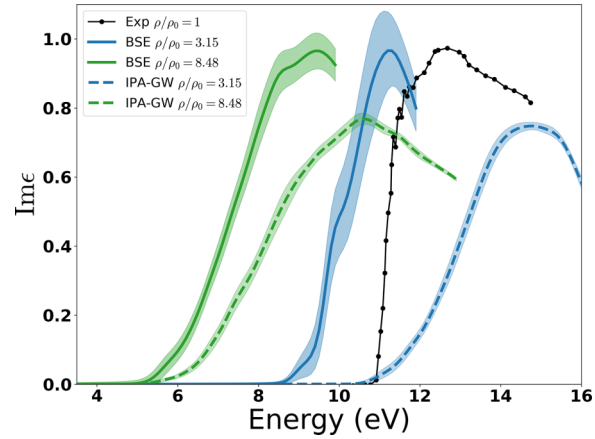

FIG. 3. Absorption spectra from BSE (solid) and IPA-GW (dashed) at $\rho/\rho_0 = 8.48$ (green) and $\rho/\rho_0 = 3.15$ (blue) and experimental spectra at $\rho/\rho_0 = 1$(black) from Ref. [63]. We have renormalized the spectra to match the experimental intensity.

the size of the supercell. In order to quantitatively correct for finite-size effects, additional information about the extension of electron-hole pairs is needed. An estimate of the excitonic length scale is $l_X = \epsilon/\mu$, where μ is the band mass describing the (extended) electron-hole excitation around the minimal gap (see the Supplemental Material [29]). Leading-order size effects of neutral excitations are then estimated as [60]

$$\Delta_n^{\infty} - \Delta_n^{L} = \max\left[\frac{|v_M(L)|}{\epsilon} - \frac{|v_M(2l_X)|}{\epsilon}, 0\right]. \quad (3)$$

For a subset of the configurations described above, we performed MBTP calculations on top of the DFT-LDA band structure. We employed both the GW and the BSE approach to compute the excitation spectra averaged over 10 configurations including both temperature and nuclear quantum effects. Whereas the GW approach addresses quasiparticle excitations, the BSE approach computes *e-h* spectra, including excitonic effects.

To have a direct comparison between the QMC and the BSE, we have performed the BSE calculations at vanishing momentum transfer. The IXS experiment measures the dynamic structure factor $S(\mathbf{q},\omega) = -q^2/(4\pi^2 n)\mathrm{Im}\epsilon_M^{-1}(\mathbf{q},\omega)$, where n is the average electron density and $\epsilon_M(\mathbf{q},\omega)$ is a macroscopic dielectric function which can be directly computed within the BSE. In our comparison to the IXS spectra, we examine the loss function at vanishing momentum: $-\lim_{\mathbf{q}\to 0}\mathrm{Im}\epsilon_M^{-1}(\mathbf{q},\omega)$. Since the excitons in solid molecular hydrogen have a Frenkel-like nature with very little dispersion [62], $\mathbf{q}\to 0$ is a good approximation of the spectral onset at finite momentum where the experiment is conducted. Note that the intensities in experimental IXS spectra are arbitrary (see the Supplemental Material [29] for theoretical and computational details). Values of the optical gap and the transition matrix elements computed using the BSE were averaged over nuclear configurations to obtain the spectra shown in Fig. 2. A 0.2-eV Gaussian broadening was applied to the final averaged spectra.

Results. We have computed quasiparticle and neutral gaps in a compression range between threefold to ninefold using both QMC and MBPT methods. Figure 1 reports our results and compares them with the experimental data of Ref. [16]. Over the whole range of compression, the system remains in the insulating state but the character of the neutral excitation changes from localized to delocalized. Quasiparticle and neutral gaps from QMC calculations are slightly larger than the GW and BSE results, respectively. For the exciton binding energies E_b (defined as the difference between the neutral/BSE and the quasiparticle/GW gaps), the agreement between QMC and MBPT methods is much better. See Table I in the the Supplemental Material [29]. A measure of localization of *e-h* pairs is the increase in the exciton binding energy from 0.5 eV at ninefold compression to 2 eV at our lowest compression.

In general, we expect the quasiparticle/GW gap to describe the onset of the continuum formed by interband transitions. A linear fit to the quasiparticle gap values extrapolates very close to the interband gap of 14.5 eV experimentally determined at zero pressure and cryogenic temperature ($\rho/\rho_0 = 1$) [63,64] and to the ionization energy of the hydrogen molecule (15 eV) [65]. The neutral/BSE gap, instead, extrapolates to the first exciton transition measured by absorption at zero pressure [63], which is only ∼0.2 eV lower than the free molecule excitation [66].

The shape of the theoretical absorption spectra from the BSE calculations shown in Fig. 3 at our lowest pressure smoothly approaches the one measured in Ref. [63] at zero pressure. Although the overall spectral structure seems to be preserved, our analysis (see Fig. 7 of the Supplemental Material [29]) shows that at our lowest density, the interband (GW) transitions start above 11 eV so that the observed lower onset of absorption in Fig. 3 is intrinsically connected to excitonic effects described by the BSE calculations. This suggests that the excitons at low compression are tightly bound [67], strongly localized on an individual molecule, supporting the

interpretation of Ref. [63] at zero pressure. At higher pressure, the binding energy decreases and the excitation becomes delocalized approaching pure interband transitions. This picture is further supported by the plot of the exciton wave function at different compressions (see Fig. 14 of the Supplemental Material [29]) [68].

In order to further support the interpretation of excitonic effects in terms of free molecular excitations at the lowest compression, we have performed QMC calculations for the neutral gap employing localized Gaussian molecular orbitals centered at each molecular center. For each configuration, the lowest gap value is obtained by considering the excitation localized on the molecule with the longest bond length, corresponding to what was found in the BSE calculations. Despite an overall offset in total energies, the value of the average gap using Gaussian molecular orbitals matches the one from our neutral calculation employing Bloch orbitals at the lowest compression. At higher compressions, this agreement is lost showing that the simple Gaussian approximation cannot describe the delocalization of the electrons in an exciton which extends over neighboring molecules.

Let us now turn to the comparison of our neutral QMC and BSE gaps with the experimental values extracted from the energy-loss edge of the IXS intensity of Ref. [16] shown in Fig. 1. We observe an excellent agreement of theory and experiment. Insight into the origin of residual deviations can be obtained by comparing the IXS and BSE spectra. In Fig. 2 we report the comparison of BSE, $-\mathrm{Im}\epsilon_M^{-1}(\mathbf{q}\to 0,\omega)$, and IXS spectra at low and high compression, together with the values of the BSE and experimentally extracted gaps indicated by vertical bars. At lower pressure/compression, the onset of energy loss is quite sharp, the BSE optical gap coincides with the observed onset in the experimental spectra. However, to eliminate background effects, the experimental gap value reported in Ref. [16] and shown in Fig. 1 is obtained by a linear extrapolation using points at higher energies. Note that deviations of the BSE calculations with respect to experimental data at higher energies are an artifact of the limited number of unoccupied bands taken into account in the BSE calculations. Possible bias due to the linear extrapolation roughly coincides with the experimental errors quoted at this compression, which must be interpreted as a systematic error. Within the BSE, the onset of energy loss is due to the sharp and intense first excitonic peak whose intensity might be larger than in experiment due to the vanishing momentum transfer in the BSE calculations (see Fig. 8 of the Supplemental Material [29]).

At higher pressure, where the excitonic intensities are weaker (see Fig. 8 of the Supplemental Material [29]), the onset is smeared out. The values of the experimental gap at higher compressions have been estimated as the intersection point between two slopes; the less steep one is attributed to residual beryllium gasket background effects (see the less steep fit of the right side of Fig. 2). In our BSE calculations, however, we observe that the IXS spectrum begins at 5.3 eV with a very weak first excitonic peak such that the BSE results are within the systematic uncertainty of the experimental gap determination.

In order to quantify the influence of thermal and quantum nuclear effects on electronic gaps we computed the gap for systems of classical protons and for the ideal $P6_3/m$ structure at the four compression values. In Fig. (4) we report Δ_{qp} for the relaxed $P6_3/m$ structure, for systems of both classical and of quantum protons at 300 K. Ideal structures have the largest gaps, thermal effects alone (classical protons) provide roughly ∼1-eV reduction of the gap while nuclear quantum effects provide an additional ∼1-eV reduction of the gap, roughly independent of compression (see the inset to Fig. 4). We expect that the deuterium gap will be halfway between the gap of hydrogen and that of classical protons. Note that we do not consider any effects of quantum statistics on the molecular rotational spectra.

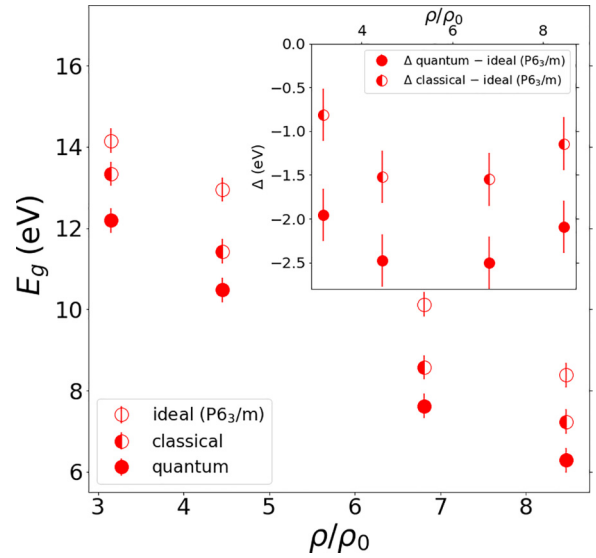

FIG. 4. Quasiparticle (QP) gap of the ideal $P6_3/m$ structure (open circles), QP gap with classical protons at room temperature (half circle), and QP gap with quantum protons at room temperature (solid circle). Inset: The reduction of the quasiparticle gap due to temperature and quantum nuclear effects (solid circles) and with only temperature effects (half-filled circles).

Conclusion. The pressure-induced variation of solid hydrogen from a wide-gap insulator towards a metal has been challenging experimentally and theoretically for decades. We have made a theoretical study of the electronic excitation gap and spectral properties based on QMC and MBPT methods of phase I where quantitative comparison to IXS measurements are possible. We have shown that quantum nuclear and excitonic effects introduce sizable reductions of the gap. In contrast to thermal and quantum nuclear effects, the reduction of the gap due to excitonic effects decreases rapidly with pressure. At our highest compression, quasiparticle/GW and neutral/BSE gaps almost coincide. Therefore, the roughly linear behavior of the closing of the gap in the range of compressions studied here and in Ref. [16] will change slope around 100 GPa to follow the line of the quasiparticle gap.

Our calculations put forward a pressure-induced crossover of the optical excitation spectra from a typical molecular crystal towards a semiconductorlike behavior. At low pressure, excitons are mainly localized on molecular centers and form

a broad excitonic band. At high compression, energy loss and absorption spectra are dominated by quasiparticle excitations with weakly bound excitons, delocalized over several unit cells. We have shown that nuclear quantum effects and intrinsic many-body calculations (MBPT or QMC) are needed for a quantitative description.

Acknowledgments. M.H. acknowledges support from the French Agency via research project SIX (ANR-23-CE30-0022). D.M.C. is supported by U.S. DOE Grant No. DE-SC0020177. C.P. was supported by the European Union - NextGenerationEU under the Italian Ministry of University and Research (MUR), Projects PRIN2022-2022NRBLPT, CUP E53D23001790006, PRIN2022-P2022MC742PNRR, CUP E53D23018440001. This research used HPC resources from GENCI-IDRIS 2022-AD010912502R1 and 2023-A0140914158 and GENCI (Project No. 544) and the GRICAD infrastructure supported by Grenoble research communities.

[1] H. K. Mao and R. Hemley, Ultrahigh-pressure transitions in solid hydrogen, Rev. Mod. Phys. **66**, 671 (1994).

[2] J. M. McMahon, M. A. Morales, C. Pierleoni, and D. M. Ceperley, The properties of hydrogen and helium under extreme conditions, Rev. Mod. Phys. **84**, 1607 (2012).

[3] E. Gregoryanz, C. Ji, P. Dalladay-Simpson, B. Li, R. T. Howie, and H.-K. Mao, Everything you always wanted to know about metallic hydrogen but were afraid to ask, Matter Radiat. Extremes **5**, 038101 (2020).

[4] P. Loubeyre, R. LeToullec, D. Hausermann, M. Hanfland, R. J. Hemley, H. K. Mao, and L. W. Finger, X-ray diffraction and equation of state of hydrogen at megabar pressures, Nature (London) **383**, 702 (1996).

[5] C. Ji, B. Li, W. Liu, J. S. Smith, A. Majumdar, W. Luo, R. Ahuja, J. Shu, J. Wang, S. Sinogeikin, Y. Meng, V. B. Prakapenka, E. Greenberg, R. Xu, X. Huang, W. Yang, G. Shen, W. L. Mao, and H.-K. Mao, Ultrahigh-pressure isostructural electronic transitions in hydrogen, Nature (London) **573**, 558 (2019).

[6] C. Ji, B. Li, W. Liu, J. S. Smith, A. Björling, A. Majumdar, W. Luo, R. Ahuja, J. Shu, J. Wang, S. Sinogeikin, Y. Meng, V. B. Prakapenka, E. Greenberg, R. Xu, X. Huang, Y. Ding, A. Soldatov, W. Yang, G. Shen *et al.*, Crystallography of low Z material at ultrahigh pressure: Case study on solid hydrogen, Matter Radiat. Extremes **5**, 038401 (2020).

[7] C. J. Pickard and R. J. Needs, Structure of phase III of solid hydrogen, Nat. Phys. **3**, 473 (2007).

[8] C. J. Pickard, M. Martinez-Canales, and R. J. Needs, Density functional theory study of phase IV of solid hydrogen, Phys. Rev. B **85**, 214114 (2012).

[9] B. Monserrat, N. D. Drummond, P. Dalladay-simpson, R. T. Howie, P. Lopez Rios, E. Gregoryanz, C. J. Pickard, and R. J. Needs, Structure and metallicity of phase V of hydrogen, Phys. Rev. Lett. **120**, 255701 (2018).

[10] P. Loubeyre, F. Occelli, and P. Dumas, Synchrotron infrared spectroscopic evidence of the probable transition to metal hydrogen, Nature (London) **577**, 631 (2020).

[11] R. P. Dias, O. Noked, and I. F. Silvera, Quantum phase transition in solid hydrogen at high pressure, Phys. Rev. B **100**, 184112 (2019).

[12] M. I. Eremets, A. P. Drozdov, P. P. Kong, and H. Wang, Semimetallic molecular hydrogen at pressure above 350 GPa, Nat. Phys. **15**, 1246 (2019).

[13] J. P. Rueff and A. Shukla, Inelastic x-ray scattering by electronic excitations under high pressure, Rev. Mod. Phys. **82**, 847 (2010).

[14] G. Shen and H. K. Mao, High-pressure studies with x-rays using diamond anvil cells, Rep. Prog. Phys. **80**, 016101 (2017).

[15] H.-K. Mao, X.-J. Chen, Y. Ding, B. Li, and L. Wang, Solids, liquids, and gases under high pressure, Rev. Mod. Phys. **90**, 015007 (2018).

[16] B. Li, Y. Ding, D. Y. Kim, L. Wang, T.-C. Weng, W. Yang, Z. Yu, C. Ji, J. Wang, J. Shu, J. Chen, K. Yang, Y. Xiao, P. Chow, G. Shen, W. L. Mao, and H.-K. Mao, Probing the electronic band gap of solid hydrogen by inelastic x-ray scattering up to 90 GPa, Phys. Rev. Lett. **126**, 036402 (2021).

[17] R. M. Martin, L. Reining, and D. M. Ceperley, *Interacting Electrons* (Cambridge University, Cambridge, England, 2016).

[18] M. Dvorak, X.-J. Chen, and Z. Wu, Quasiparticle energies and excitonic effects in dense solid hydrogen near metallization, Phys. Rev. B **90**, 035103 (2014).

[19] S. Lebegue, C. M. Araujo, D. Y. Kim, M. Ramzan, H.-k. Mao, and R. Ahuja, Semimetallic dense hydrogen above 260 GPa, Proc. Natl. Acad. Sci. USA **109**, 9766 (2012).

[20] S. Azadi, A. Davydov, and E. Kozik, *GW* space-time method: Energy band gap of solid hydrogen, Phys. Rev. B **105**, 155136 (2022).

[21] E. Kioupakis, P. Zhang, M. L. Cohen, and S. G. Louie, *GW* quasiparticle corrections to the LDA $+ U$/GGA $+ U$ electronic structure of bcc hydrogen, Phys. Rev. B **77**, 155114 (2008).

[22] V. Gorelov, M. Holzmann, D. M. Ceperley, and C. Pierleoni, Energy gap closure of crystalline molecular hydrogen with pressure, Phys. Rev. Lett. **124**, 116401 (2020).

[23] V. Gorelov, D. M. Ceperley, M. Holzmann, and C. Pierleoni, Electronic energy gap closure and metal-insulator transition in dense liquid hydrogen, Phys. Rev. B **102**, 195133 (2020).

[24] S. Azadi, N. D. Drummond, and W. M. C. Foulkes, Nature of the metallization transition in solid hydrogen, Phys. Rev. B **95**, 035142 (2017).

[25] L. Monacelli, M. Casula, K. Nakano, S. Sorella, and F. Mauri, Quantum phase diagram of high-pressure hydrogen, Nat. Phys. **19**, 845 (2023).

[26] H. Niu, Y. Yang, S. Jensen, M. Holzmann, C. Pierleoni, and D. M. Ceperley, Stable solid molecular hydrogen above 900 K from a machine-learned potential trained with diffusion quantum Monte Carlo, Phys. Rev. Lett. **130**, 076102 (2023).

[27] R. C. Clay, J. Mcminis, J. M. McMahon, C. Pierleoni, D. M. Ceperley, and M. A. Morales, Benchmarking exchange-correlation functionals for hydrogen at high pressures using quantum Monte Carlo, Phys. Rev. B **89**, 184106 (2014).

[28] V. Gorelov, C. Pierleoni, and D. M. Ceperley, Benchmarking vdW-DF first-principles predictions against coupled electron–ion Monte Carlo for high-pressure liquid hydrogen, Contrib. Plasma Phys. **59**, e201800185 (2019).

[29] See Supplemental Material at http://link.aps.org/supplemental/10.1103/PhysRevB.109.L241111 for the details of the calculations performed, theoretical background of the methods used, and convergence studies.

[30] M. Holzmann, D. M. Ceperley, C. Pierleoni, and K. Esler, Backflow correlations for the electron gas and metallic hydrogen, Phys. Rev. E **68**, 046707 (2003).

[31] C. Pierleoni, K. T. Delaney, M. A. Morales, D. M. Ceperley, and M. Holzmann, Trial wave functions for high-pressure metallic hydrogen, Comput. Phys. Commun. **179**, 89 (2008).

[32] P. Giannozzi, S. Baroni, N. Bonini, M. Calandra, R. Car, C. Cavazzoni, D. Ceresoli, G. L. Chiarotti, M. Cococcioni, I. Dabo, A. D. Corso, S. de Gironcoli, S. Fabris, G. Fratesi, R. Gebauer, U. Gerstmann, C. Gougoussis, A. Kokalj, M. Lazzeri, L. Martin-Samos *et al.*, QUANTUM ESPRESSO: a modular and open-source software project for quantum simulations of materials, J. Phys.: Condens. Matter **21**, 395502 (2009).

[33] P. Giannozzi, O. Andreussi, T. Brumme, O. Bunau, M. B. Nardelli, M. Calandra, R. Car, C. Cavazzoni, D. Ceresoli, M. Cococcioni, N. Colonna, I. Carnimeo, A. D. Corso, S. de Gironcoli, P. Delugas, R. A. DiStasio, A. Ferretti, A. Floris, G. Fratesi, G. Fugallo *et al.*, Advanced capabilities for materials modelling with QUANTUM ESPRESSO, J. Phys.: Condens. Matter **29**, 465901 (2017).

[34] M. Morales, R. Clay, C. Pierleoni, and D. Ceperley, First principles Methods: A perspective from quantum Monte Carlo, Entropy **16**, 287 (2013).

[35] C. Pierleoni, M. a. Morales, G. Rillo, M. Holzmann, and D. M. Ceperley, Liquid–liquid phase transition in hydrogen by coupled electron–ion Monte Carlo simulations, Proc. Natl. Acad. Sci. USA **113**, 4953 (2016).

[36] F. E. Williams, An absolute theory of solid-state luminescence, J. Chem. Phys. **19**, 457 (1951).

[37] M. Lax, The Franck-Condon principle and its application to crystals, J. Chem. Phys. **20**, 1752 (1952).

[38] J. H. Constable, C. F. Clark, and J. R. Gaines, The dielectric constant of H_2, D_2, and HD in the condensed phases, J. Low Temp. Phys. **21**, 599 (1975).

[39] A. Annaberdiyev, G. Wang, C. A. Melton, M. C. Bennett, and L. Mitas, Cohesion and excitations of diamond-structure silicon by quantum Monte Carlo: Benchmarks and control of systematic biases, Phys. Rev. B **103**, 205206 (2021).

[40] Y. Yang, V. Gorelov, C. Pierleoni, D. M. Ceperley, and M. Holzmann, Electronic band gaps from quantum Monte Carlo methods, Phys. Rev. B **101**, 085115 (2020).

[41] D. M. Ceperley and B. J. Alder, Ground state of solid hydrogen at high pressures, Phys. Rev. B **36**, 2092 (1987).

[42] G. Onida, L. Reining, and A. Rubio, Electronic excitations: density-functional versus many-body Green's-function approaches, Rev. Mod. Phys. **74**, 601 (2002).

[43] G. Strinati, Application of the Green's functions method to the study of the optical properties of semiconductors, Riv. Nuovo Cimento **11**, 1 (1988), and references therein.

[44] L. Hedin, New method for calculating the one-particle Green's function with application to the electron-gas problem, Phys. Rev. **139**, A796 (1965).

[45] S. L. Adler, Quantum theory of the dielectric constant in real solids, Phys. Rev. **126**, 413 (1962).

[46] N. Wiser, Dielectric constant with local field effects included, Phys. Rev. **129**, 62 (1963).

[47] M. S. Hybertsen and S. G. Louie, Electron correlation in semiconductors and insulators: Band gaps and quasiparticle energies, Phys. Rev. B **34**, 5390 (1986).

[48] R. W. Godby, M. Schlüter, and L. J. Sham, Self-energy operators and exchange-correlation potentials in semiconductors, Phys. Rev. B **37**, 10159 (1988).

[49] S. Albrecht, L. Reining, R. Del Sole, and G. Onida, *Ab initio* calculation of excitonic effects in the optical spectra of semiconductors, Phys. Rev. Lett. **80**, 4510 (1998).

[50] L. X. Benedict, E. L. Shirley, and R. B. Bohn, Optical absorption of insulators and the electron-hole interaction: An *ab initio* calculation, Phys. Rev. Lett. **80**, 4514 (1998).

[51] M. Rohlfing and S. G. Louie, Electron-hole excitations and optical spectra from first principles, Phys. Rev. B **62**, 4927 (2000).

[52] X. Gonze, G.-M. Rignanese, M. Verstraete, J.-M. Beuken, Y. Pouillon, R. Caracas, F. Jollet, M. Torrent, G. Zerah, M. Mikami *et al.*, A brief introduction to the ABINIT software package, Z. Kristallogr **220**, 558 (2005).

[53] http://www.bethe-salpeter.org/.

[54] F. Hüser, T. Olsen, and K. S. Thygesen, Quasiparticle GW calculations for solids, molecules, and two-dimensional materials, Phys. Rev. B **87**, 235132 (2013).

[55] V. Gorelov, L. Reining, W. R. L. Lambrecht, and M. Gatti, Robustness of electronic screening effects in electron spectroscopies: Example of V_2O_5, Phys. Rev. B **107**, 075101 (2023).

[56] V. Gorelov, L. Reining, M. Feneberg, R. Goldhahn, A. Schleife, W. R. L. Lambrecht, and M. Gatti, Delocalization of dark and bright excitons in flat-band materials and the optical properties of V_2O_5, npj Comput. Mater. **8**, 94 (2022).

[57] V. Gorelov, D. M. Ceperley, M. Holzmann, and C. Pierleoni, Electronic structure and optical properties of quantum crystals from first principles calculations in the Born-Oppenheimer approximation, J. Chem. Phys. **153**, 234117 (2020).

[58] G. Makov and M. C. Payne, Periodic boundary conditions in *ab initio* calculations, Phys. Rev. B **51**, 4014 (1995).

[59] G. E. Engel, Y. Kwon, and R. M. Martin, Quasiparticle bands in a two-dimensional crystal found by *GW* and quantum Monte Carlo calculations, Phys. Rev. B **51**, 13538 (1995).

[60] V. Gorelov, Y. Yang, M. Ruggeri, D. M. Ceperley, C. Pierleoni, and M. Holzmann, Neutral band gap of carbon by quantum Monte Carlo methods, Condens. Matter Phys. **26**, 33701 (2023).

[61] R. J. Hunt, M. Szyniszewski, G. I. Prayogo, R. Maezono, and N. D. Drummond, Quantum Monte Carlo calculations of energy gaps from first principles, Phys. Rev. B **98**, 075122 (2018).

[62] P. Cudazzo, M. Gatti, A. Rubio, and F. Sottile, Frenkel versus charge-transfer exciton dispersion in molecular crystals, Phys. Rev. B **88**, 195152 (2013).

[63] K. Inoue, H. Kanzaki, and S. Suga, Fundamental absorption spectra of solid hydrogen, Solid State Commun. **30**, 627 (1979).

[64] P. Loubeyre, F. Occelli, and R. LeToullec, Optical studies of solid hydrogen to 320 GPa and evidence for black hydrogen, Nature (London) **416**, 613 (2002).

[65] H. Beutler and H. O. Junger, Uber das Absorptionsspektrum des Wasserstoffs. III, Z. Phys. **100**, 80 (1936).

[66] G. Herzberg, *Molecular Spectra and Molecular Structure. Volume I: Spectra of Diatomic Molecules*, 2nd ed. (D. Van Nostrand, New York, NY, 1950), p. 658.

[67] A. S. Davydov, *Theory of Molecular Excitons*, 1st ed. (Springer, New York, 1971), p. 313.

[68] We have verified that the first exciton energies in absorption spectra are identical to those in the energy-loss spectra.